



**A new  
electrodynamic  
balance design for  
low temperature  
studies**

H.-J. Tong et al.

# A new electrodynamic balance design for low temperature studies

H.-J. Tong<sup>1</sup>, B. Ouyang<sup>1</sup>, F. D. Pope<sup>2</sup>, and M. Kalberer<sup>1</sup>

<sup>1</sup>Centre for Atmospheric Science, University of Cambridge, Lensfield Road, Cambridge, CB2 1EW, UK

<sup>2</sup>School of Geography, Earth and Environmental Sciences, University of Birmingham, Edgbaston, Birmingham, B15 2TT, UK

Received: 17 June 2014 – Accepted: 2 July 2014 – Published: 28 July 2014

Correspondence to: F. D. Pope (f.pope@bham.ac.uk)

Published by Copernicus Publications on behalf of the European Geosciences Union.

Title Page

Abstract

Introduction

Conclusions

References

Tables

Figures



Back

Close

Full Screen / Esc

Printer-friendly Version

Interactive Discussion



## Abstract

In this paper we describe a newly designed cold electrodynamic balance (CEDB) system, which was built to study the evaporation kinetics and freezing properties of supercooled water droplets. The temperature of the CEDB chamber at the location of the levitated water droplet can be controlled in the range:  $-40$  to  $+40$  °C, which is achieved using a combination of liquid nitrogen cooling and heating by positive temperature coefficient heaters. The measurement of liquid droplet radius is obtained by analyzing the Mie elastic light scattering from a 532 nm laser. The Mie scattering signal was also used to characterize and distinguish droplet freezing events; liquid droplets produce a regular fringe pattern whilst the pattern from frozen particles is irregular. The evaporation rate of singly levitated water droplets was calculated from time resolved measurements of the radii of evaporating droplets and a clear trend of the evaporation rate on temperature was measured. The statistical freezing probabilities of aqueous pollen extracts (pollen washing water) are obtained in the temperature range:  $-4.5$  to  $-40$  °C. It was found that that pollen washing water from water birch (*Betula fontinalis occidentalis*) pollen can act as ice nuclei in the immersion freezing mode at temperatures as warm as  $-22.45$  ( $\pm 0.65$ ) °C.

## 1 Introduction

At subzero temperatures, water is observed in clouds as both supercooled water droplets (SWD) and ice particles (Mason, 1975; Cantrell and Heymsfield, 2005). In the absence of ice nuclei (IN), cloud droplets can be supercooled down to temperatures that approach the homogeneous freezing point  $\sim -38$  °C which is dependent on droplet size (Sassen, 1985; Rauber and Tokay, 1991; Hogan et al., 2004). The evaporation kinetics, and hence droplet size, of SWD influences the lifetime and radiative properties of clouds and in particular mixed-phase clouds; it can also affect the likelihood and rate of precipitation (Rosenfeld and Woodley, 2000; Lohmann and Feichter, 2005).

### A new electrodynamic balance design for low temperature studies

H.-J. Tong et al.

Title Page

Abstract

Introduction

Conclusions

References

Tables

Figures

◀

▶

◀

▶

Back

Close

Full Screen / Esc

Printer-friendly Version

Interactive Discussion



## A new electrodynamic balance design for low temperature studies

H.-J. Tong et al.

Title Page

Abstract

Introduction

Conclusions

References

Tables

Figures

◀

▶

◀

▶

Back

Close

Full Screen / Esc

Printer-friendly Version

Interactive Discussion



At temperatures above the homogenous freezing point, the heterogeneous freezing of SWD is caused by interaction of IN active aerosols with SWD. Several distinct mechanisms exist, including: the deposition, immersion, condensation, and contact modes of freezing (Prupacher and Klett, 1997). Recently there has been an intense research effort to determine the efficiencies and relevance of the different modes of freezing (e.g. Murray et al., 2010; Knopf et al., 2011; Crawford et al., 2011; Kanji et al., 2013; Hoffmann et al., 2013a; Atkinson et al., 2013.) Summaries of previous results, obtained by both laboratory and field work, and the atmospheric implications of these studies are provided by several recent review articles and no further detail is given here (Laaksonen et al., 1995; Pöschl, 2005; Hoose and Möhler, 2012; Murray et al., 2012; Ladino Moreno et al., 2013). It is noted that several studies suggest that IN processes are still not sufficiently understood for satisfactory global modelling (e.g. Hoose et al., 2010; DeMott et al., 2010). The most important types of aerosol particles to act as IN are reported to be mineral dust and primary biological aerosols (PBA), with these two aerosol groups accounting for more than 80 % of ice-crystal residues (Pratt et al., 2009). PBA are typically large in size (mainly supermicron) and they often dominate the measured mass loading of atmospheric aerosol. However, their number density concentration is small and usually dwarfed by other aerosol types except in the most pristine environments (Griffiths et al., 2012). PBA species include: pollen, bacteria, fungal, algae, moss and fern spores, viruses and fragments of animals and plants (Deguillaume et al., 2008; Moller et al., 2008; Després et al., 2007; Möhler et al., 2007). The atmospheric transport, and hence dispersal, of pollen requires meteorological conditions to produce uplift of pollen containing air. Atmospheric removal of pollen is determined by the wet and dry deposition rates. The dry deposition is controlled by the settling speed of the pollen grain which is a function of particle density and size (Aylor, 2002). Both computer modelling and field studies have shown that pollen is capable of travelling large distances and can remain airborne on the order of days (Rousseau et al., 2003; Sofiev et al., 2006; Helbig et al., 2004; Heise and Heise, 1948).

## A new electrodynamic balance design for low temperature studies

H.-J. Tong et al.

Title Page

Abstract

Introduction

Conclusions

References

Tables

Figures

◀

▶

◀

▶

Back

Close

Full Screen / Esc

Printer-friendly Version

Interactive Discussion

Previous work in our group has used the environmental scanning electron microscope (ESEM) and warm EDB systems to measure the hygroscopicity and hence the warm cloud condensation nuclei (CCN) ability of pollen grains (Pope, 2010; Griffiths et al., 2012). Within liquid water, such as in rain droplets, pollen grains are observed to burst thereby releasing smaller material, such as sugars, macromolecules and allergens, into solution (Yttri et al., 2007; Schäppi et al., 1999; Pummer et al., 2012; Augustin et al., 2013).

Pollen grains have been found to be IN active. Within the condensation freezing mode pollen can initiate freezing events at temperatures up to  $-8^{\circ}\text{C}$  (Diehl et al., 2001), within the immersion freezing mode at temperatures up to  $-9^{\circ}\text{C}$  (Diehl et al., 2002), and within the contact freezing mode up to  $-5^{\circ}\text{C}$  (Diehl et al., 2002). Furthermore, it is found that water that has interacted with pollen grains can also be IN active in the immersion mode of freezing. This water is referred to as pollen washing water (PWW). In particular, suspended macromolecules within PWW were identified as efficient IN (Pummer et al., 2012; Augustin et al., 2013). Work by the group of Grothe has used two distinct techniques to assess the IN ability of PWW ensembles: firstly freezing events of PWW droplets that are held within emulsions can be observed through use of a microscope fitted with a cryostage (Pummer et al., 2012). Secondly the Leipzig Aerosol Cloud Interaction Simulator (LACIS, Stratman et al.; 2004) technique is utilized (Augustin et al., 2013). These results indicate high IN efficiency of PWW in the immersion mode up to  $-16^{\circ}\text{C}$ .

As a robust methodology for the levitation of single particles which carry electric charge, the electrodynamic balance (EDB) technique has been applied in atmosphere science for several decades (see reviews by Davis, 1997; Krieger et al., 2012). On the base of such a strategy, numerous work has been carried out on aerosol particles and droplets, including but not limited to: contact ion pairs formation (e.g. Zhang and Chan, 2000; Lee et al., 2008), hygroscopicity and phase transition (e.g. Tang and Munkelwitz, 1994; Choi and Chan, 2002; Li et al., 2005; Parsons et al., 2006; Pope et al., 2010a), measurement of vapour pressure (e.g. Pope et al., 2010b; Soonsin

---

## A new electrodynamic balance design for low temperature studies

H.-J. Tong et al.

---

Title Page

Abstract

Introduction

Conclusions

References

Tables

Figures

◀

▶

◀

▶

Back

Close

Full Screen / Esc

Printer-friendly Version

Interactive Discussion



et al., 2010), oxidation chemistry (e.g. Lee and Chan, 2007; Pope et al., 2010c; Lee et al., 2012), and supercooled droplets and ice nucleation (e.g. Swanson et al., 1999; Krieger et al., 2000; Svensson et al., 2009; Hoffmann et al., 2013b). Recently, a new EDB design with concentric cylindrical electrodes was developed to measure rapid evaporation and condensation process of single droplets (Heinisch et al., 2006, 2009; Davies et al., 2011, 2013). Using a similar EDB design to Heinisch et al., we developed and incorporated a new cooling system which is applicable for low temperature studies. The design was chosen because the cylindrical electrodes are mechanically stable and single droplets can be stably confined within a small and well defined null point region of the electrodynamic balance whilst gas flows ( $> 100$  sccm) are directed past the droplet (Heinisch et al., 2006; Davies et al., 2011). We describe the new cold EDB (CEDB) system providing particular detail on the cooling strategy. Furthermore, we provide measurement data, from the first applications of this new system: the evaporation rates of supercooled droplets, and the freezing ability of these droplets with and without PWW present. In particular this study provides the first contact free measurements of ice nucleation of individual PWW droplets.

## 2 Design and characterisation of new CEDB

The schematic diagram of the new CEDB system is shown in Fig. 1. The system is capable of trapping droplets and following the evolution of the droplet radius under well-defined conditions of temperature and humidity. The evaporation and freezing processes of droplets can also be distinguished by following the Mie scattering phase function. The detailed experimental procedure and analysis strategy is now detailed.

### 2.1 Droplet trapping and sizing

The details of the geometrical structure of the EDB chamber, AC and DC electrodes, and the theoretical calculation on the electrodynamic field generated have been

## A new electrodynamic balance design for low temperature studies

H.-J. Tong et al.

Title Page

Abstract

Introduction

Conclusions

References

Tables

Figures

◀

▶

◀

▶

Back

Close

Full Screen / Esc

Printer-friendly Version

Interactive Discussion

reported previously by Heinisch et al. (2009) and Davies et al. (2012) and will be discussed only briefly here. The cylindrical electrodes are composed of four electrodes: two upper and two lower. Both the upper and lower electrodes consist of a pair of inner (①) and outer (②) electrodes as shown in Fig. 1. Both the outer electrodes are grounded. The upper-inner electrode has a combined DC and AC input ( $V_{AC} + V_{DC}$ ). The DC voltage can be varied between  $-200-0$  V, the AC voltage between  $0-1$  kV with a high speed and high voltage amplifier module (AP-1B3, Matsusada Precision Inc.), and the AC frequency between  $10-300$  Hz. The lower-inner electrode has the same AC input applied to it as the upper-inner electrode but without the DC coupling. Both of the inner electrodes were insulated from the outer electrodes through use of a thin rubber insulator. Droplets were delivered into the CEDB using a droplet dispenser, which is optimized for low temperature conditions, (MicroFab,  $30\ \mu\text{m}$  orifice diameter, MJ-ABP-01). When the same dispenser parameter settings (pulse width, frequency and amplitude etc.) are used the generated droplets are of high reproducibility with radius fluctuation smaller than  $0.5\ \mu\text{m}$ . Within this study the use of different parameter settings led to slight differences in initial SWD size. From the dispenser the droplets follow a trajectory past a charging electrode which is held at  $900$  V (generated from a Brandenburg 476R high voltage photomultiplier power supply) thereby allowing the droplet to pick up sufficient charge for trapping. Subsequent to the charging electrode, the droplets pass into the centre of the CEDB chamber where the droplets are trapped in the null point of the electrodynamic field.

The procedure for the size calibration of the droplet is the same as we previously used (Pope et al., 2010b). A cw  $532\ \text{nm}$  wavelength laser (532GLM20, Changchun Dragon Lasers Co., Ltd), with a power of  $\sim 20$  mW, illuminates the trapped spherical droplet thus generating Mie scattering resonances. These resonances were recorded over a  $21^\circ$  window, as measured by the angle subtended from the null point to the edges of the window port, using a monochrome complementary metal oxide semiconductor camera (Thorlabs, DCC1545M) centred at  $\sim 135^\circ$  relative to the forward direction of the laser. The particle size obtained by Mie scattering was calibrated using dry lime

soda glass sphere standards of the following diameters:  $19.3 \pm 1.0$ ,  $30.1 \pm 1.1$ ,  $42.3 \pm 1.0 \mu\text{m}$  (Thermo Scientific Duke Standards, 9020, 9030, 9040). The particle size was determined by applying the calculation shown in Eq. (1) (Glantschnig and Chen, 1981), which is based on Mie theory (Mie, 1908), to the experimentally determined peak-to-peak average of the recorded resonances.

$$\Delta\theta \cong \frac{\lambda}{r} \left( \cos \frac{\theta}{2} + \frac{n \sin \frac{\theta}{2}}{\sqrt{1 + n^2 - 2n \cos \frac{\theta}{2}}} \right)^{-1} \quad (1)$$

In Eq. (1)  $\lambda$  is the illuminating laser wavelength (532 nm).  $n$  is the refractive index of trapped droplet (1.33 will be used in this study for pure water),  $\theta$  is the median angle of observed phase functions,  $r$  is the droplet radius, and  $\Delta\theta$  is the angular separation. The excellent agreement between the experimental calibration data and the theoretical calculations are shown in Fig. 2. Labview software was used for experimental control and data acquisition.

## 2.2 Cooling strategy of CEDB

To cool the CEDB system, a liquid nitrogen Dewar was attached to the top of the CEDB. This Dewar consists of double walled liquid nitrogen reservoir with a vacuum held between the two walls. To further reduce heat exchange between the liquid nitrogen Dewar and the ambient atmosphere, the outer surface of the liquid nitrogen cylinder is covered with flexible synthetic rubber insulation (Insul-tube and Insul-sheet, NMC (UK) Ltd) with a thickness of  $\sim 9$  mm. The top of the Dewar is sealed with a Polytetrafluoroethene (PTFE) cap which is also insulated with synthetic rubber. The vacuum and insulation material significantly reduce the evaporation of liquid nitrogen thereby increasing the temperature stability within the CEDB chamber.

The CEDB chamber is cooled by flowing  $\text{N}_2$  gas through two copper heat exchange pipes (3 mm outside diameter). The pipes pass through the liquid nitrogen Dewar and

## A new electrodynamic balance design for low temperature studies

H.-J. Tong et al.

Title Page

Abstract

Introduction

Conclusions

References

Tables

Figures

◀

▶

◀

▶

Back

Close

Full Screen / Esc

Printer-friendly Version

Interactive Discussion



## A new electrodynamic balance design for low temperature studies

H.-J. Tong et al.

Title Page

Abstract

Introduction

Conclusions

References

Tables

Figures

◀

▶

◀

▶

Back

Close

Full Screen / Esc

Printer-friendly Version

Interactive Discussion

direct the gas flows through the upper electrodes (see Fig. 1). The gas flow from the central pipe passes through the upper-inner electrode and directly passes through the null point region of the CEDB. The gas flow from the outer pipe is directed through the gap formed between the inner and outer-upper electrodes and acts as an additional cooling sheath gas. The gas flows are controlled using mass flow controllers (Brooks Smart MFC, Brooks Instruments) and are set to  $\sim 80$  sccm for the outer pipe (MFC 1 in Fig. 1) and 20 sccm for the central pipe (MFC 2 in Fig. 1). The flow rates are both laminar and matched in downward velocity. The Reynolds number of the two gas flows, can be calculated with Eq. (2), where  $d$  is diameter of inner (0.002 m) or outer electrode (0.004 m).  $u$  is the mass flow velocity ( $\text{m s}^{-1}$ ).  $\rho$  is the density ( $1.13 \text{ kg m}^{-3}$  for nitrogen gas).  $\eta$  is the dynamic viscosity ( $1.75 \times 10^{-5} \text{ Pa s}$  for nitrogen gas at  $20^\circ\text{C}$ ). The calculated Reynolds numbers at  $20^\circ\text{C}$  are 27.4 and 13.7 for the 80 and 20 sccm flow rates, respectively. These low Reynolds numbers comfortably ensure laminar flow at all temperatures investigated in this study.

$$Re = \frac{d u \rho}{\eta} \quad (2)$$

The temperature at the null point of the CEDB is controlled by varying the temperature of the CEDB chamber wall using variable heaters (HP05-1/10-24, Onecall). The null point temperature and radial temperature gradient are measured using a  $0.1^\circ\text{C}$  resolution thermometer (HH 308, Omega) with type K thermocouples. A temperature calibration curve for the null point position is shown in Fig. 3a. It can be seen that the null point temperature varies linearly with the DC voltage that is supplied to the heater. This configuration allows for easy control of the null point temperature between  $-40$ – $0^\circ\text{C}$ . When insulating all the 8 outer metal surfaces of the CEDB chamber with 4 mm depth rubber insulator, the null point temperature can be controlled from  $-30$  to  $-42^\circ\text{C}$  with a heating range from 17 to 38 V. If only 6 outer metal surfaces are insulated, the null point temperature can be regulated from  $40$  to  $-31^\circ\text{C}$  with a heating range from 24 to 43 V. Only the calibration curve ranges from 5 to  $-42^\circ\text{C}$  are shown in Fig. 3. This



## A new electrodynamic balance design for low temperature studies

H.-J. Tong et al.

Title Page

Abstract

Introduction

Conclusions

References

Tables

Figures

◀

▶

◀

▶

Back

Close

Full Screen / Esc

Printer-friendly Version

Interactive Discussion



configuration sets up a radial temperature gradient within the cell at the height of the null point. The radial temperature gradients are  $< 1\text{ }^{\circ}\text{C mm}^{-1}$  along the horizontal axis and  $< 1.5\text{ }^{\circ}\text{C mm}^{-1}$  along the vertical axis. The relative humidity at the null point can get  $< 0.2\%$  (EK-H5 kit with SHT75 Humidity sensor, Sensirion) when the temperature is higher than  $-20\text{ }^{\circ}\text{C}$ , and  $< 0.7\%$  when the temperature reaches  $\sim -40\text{ }^{\circ}\text{C}$ . Figure 3b provides an example of the time required for the temperature of both the CEDB null point and the outer glass window surface to reach steady state.

In order to stop the formation of condensation and or freezing on the outer surface of the glass windows (Knight Optical BK7), a rubber insulator (⑥ in Fig. 1) was used between the window and metal body of the chamber. Furthermore, the outer surface of the glass window was warmed by a heating jacket (④ in Fig. 1). The jacket was designed so the outside face of the window could be exposed to the laboratory air. Such a design allows for the easy alignment of the laser into the chamber and through the CEDB null point. When the outside surface temperature of the glass windows was lower than  $15\text{ }^{\circ}\text{C}$ , a dry laminar air flow is also directed onto the surface to avoid water condensation and to maintain the transparency of the window.

### 3 Results and discussion

The first applications of the new CEDB system, detailed in this paper, are in the study of the evaporation kinetics of SWD and the immersion freezing ability of PWW droplets.

#### 3.1 Evaporation kinetics of supercooled water droplets

As the main application of the CEDB will be the investigation of freezing events of aqueous droplets it is necessary to characterise the evaporation rate of SWD, which defines the time window accessible for the freezing studies. To ensure that the nitrogen gas was as dry as possible, the flow from the cylinder was passed through a 30 cm long, and 5 cm in diameter, drying tube containing silica gel particles (Breckland Scientific

## A new electrodynamic balance design for low temperature studies

H.-J. Tong et al.

Title Page

Abstract

Introduction

Conclusions

References

Tables

Figures

◀

▶

◀

▶

Back

Close

Full Screen / Esc

Printer-friendly Version

Interactive Discussion

Supplies Ltd). Any remaining water vapour in the gas flow is caught in the cold trap formed by copper tubing heat exchangers which are held at near liquid nitrogen temperature ( $-196^{\circ}\text{C}$ ). Considering the saturation vapour pressures of liquid water and ice at  $\sim -150^{\circ}\text{C}$  (123 K) are  $3.02 \times 10^{-9}$  and  $8.50 \times 10^{-10}$  Pa, and the vapour pressure is decreasing as the temperature is lowering (Murphy and Koop, 2005), we assume that the evaporation of SWD in the present study occurs under a dry environment. HPLC grade water (RH1020, Rathburn Chemicals Ltd.) was used to generate the water droplets. Pure water droplets were only injected into the CEDB chamber once the null point temperature had stabilized to the desired temperature. The evaporation rate of SWD recorded at  $-18.8 (\pm 0.6)$ ,  $-22.7 (\pm 0.6)$ ,  $-28.0 (\pm 0.6)$ ,  $-32.1 (\pm 0.6)$  and  $-34.2 (\pm 0.6)^{\circ}\text{C}$ , as measured by the change in radius, are shown in Fig. 4a. This figure indicates that under dry nitrogen gas flow the evaporation rate of SWD decreases as temperature of the null point decreases, as expected, because of the decreasing water vapour pressure. The evaporation rate of SWD can be parameterized by determining the time taken for the droplet to evaporate to half of its initial radius ( $t_{r1/2}$ ). An alternative parameterization is the ratio of  $t_{r1/2}$  to the initial radius of the droplet ( $t_{r1/2}/R$ ) which minimises the influence of initial SWD size fluctuation (Fig. 4b). This parameterization strategy has been previously used as an empirical tool to estimate the mass transfer of water molecules in glassy aerosol droplets (Tong et al., 2011).

Conclusively, the CEDB data indicate that water droplets with a radius of  $\sim 15 \mu\text{m}$  can be trapped for ca. 10–60 s within a  $\sim 100$  sccm pure nitrogen gas in the temperature range from  $-5.7$  to  $-34.5^{\circ}\text{C}$ , thus defining the time scale available for freezing experiments in the current CEDB set up.

The mean free path of  $\text{N}_2$  gas ( $\lambda_{\text{N}_2}$ ) at subzero temperatures and atmospheric pressure is less than 58.8 nm (Hirschfelder et al., 1954). Considering that the measured droplet radius ( $r$ ) is always greater than  $2.5 \mu\text{m}$ , then the Knudsen number,  $Kn = \lambda_{\text{N}_2}/r$ , is always much smaller than 1. Hence the  $\text{N}_2$  gas flow is always in the continuum regime (Seinfeld and Pandis, 1998), and we estimate the mass transfer of water molecules from the SWD surface to the surrounding  $\text{N}_2$  atmosphere may be a significant factor

as well as the heat transfer to influence SWD's kinetic evaporation rate (Miles et al., 2012; Holyst et al., 2013). Although in this study we do not quantify the influence of mass and heat transfer on the evaporating rate of SWDs, these results show that SWD evaporation kinetics can be measured, in the new CEDB, at temperatures approaching the homogenous freezing temperature. This study will form the basis of a forthcoming paper.

### 3.2 Immersion freezing of PWW solution

The extraction procedure for the PWW solutions, which is illustrated in Fig. 5a, is similar to the procedure used by Augustin et al. (2013). Briefly, water birch pollen (*Betula fontinalis occidentalis*), which was obtained as a dried sample from Sigma–Aldrich (P6895-1G), were suspended in water at a mass concentration of 5 g ml<sup>-1</sup> and stirred for ~ 1 min using a mixer (Fisher Scientific Top Mix FB 15024). After stirring, the suspension was then stored in a fridge for 24 h. The solution was then stirred again and filtered through sequential use of 0.45 and 0.2 μm pore filters (Supelco, 4 mm, PTFE membrane). In this aspect the procedure differed from that of Augustin et al. which used filters of size 4–7 μm. After the filtration, the PWW solution is observed to be transparent but with a bright yellow hue. Each filtered PWW solution was used within 4 days of preparation to minimize the risk of contamination. The mass fraction ( $f_{PWW}$ ) of biological material within the PWW solution is obtained by measuring the mass of the extracted PWW solution and mass of the dried residue with a 0.1 mg accuracy balance (Fisherbrand PS-60). Dry PWW residues were obtained by evaporating the PWW solutions under nitrogen gas (Air liquid UK limited, > 99.999 %) and subsequent heating within an oven (Mettler, ULM 400) at a temperature < 95 °C for more than 4 h.

Figure 6 provides the calibration curve for the mass fraction of biological material in solution vs. initial concentration of pollen mass in the extraction solution. Furthermore, the refractive index of the PWW solution is measured using a refractometer (RFM340, Bellingham + Stanley Ltd.), also shown in Fig. 6.

**A new  
electrodynamic  
balance design for  
low temperature  
studies**

H.-J. Tong et al.

Title Page

Abstract

Introduction

Conclusions

References

Tables

Figures

◀

▶

◀

▶

Back

Close

Full Screen / Esc

Printer-friendly Version

Interactive Discussion



## A new electrodynamic balance design for low temperature studies

H.-J. Tong et al.

Title Page

Abstract

Introduction

Conclusions

References

Tables

Figures

◀

▶

◀

▶

Back

Close

Full Screen / Esc

Printer-friendly Version

Interactive Discussion



Figure 6 clearly indicates that the mass fraction of PWW solutions ( $f_{\text{PWW}}$ ) increase from 0.000135–0.0129 as the pollen suspension concentration ( $W_{\text{pollen}}$ ) increases from 1–50 mg ml<sup>-1</sup> (pollen mass per water volume). The upper threshold,  $f_{\text{PWW}} = 0.0129$ , in this study is similar to mass fractions used in the study of Pummer et al. (2012). However, within the experiments described in this study, the values of  $f_{\text{PWW}}$  will increase as the water content of the PWW droplets evaporate. The refractive index of PWW solutions ( $RI_{\text{PWW}}$ ) increase from 1.332905 (pure water) to 1.33543 as the pollen suspension concentration increase from 0 to 50 mg ml<sup>-1</sup>. To calculate the particle size, via equation E2, we used the refractive index value of pure water ( $n = 1.33$ ) in all cases. For a 15 μm (in radius) PWW droplet, without considering the density evolution of it during the evaporation process, at most this simplification led to an overestimation of the initial droplet size by ~ 0.28 %, and 0.54 % for the same droplet at time  $t_{r1/2}$ .

Freezing events of the PWW droplets are identified by the change in the elastic Mie scattering signal. Liquid droplets are spherical and produce regular fringe patterns, whilst frozen solid particles are non-spherical and produce irregular patterns. Such a strategy for distinguishing liquid and frozen droplets has been successfully demonstrated previously (e.g. Krämer et al., 1999; Shaw et al., 1999; Vortisch et al., 2000). Examples of different phase functions are shown in Fig. 5b–e. In particular, Fig. 5b provides images of scattered light recorded at 1.3 and 10 s, respectively, after capture in the EDB trap from a PWW droplet at  $-21.8^{\circ}\text{C}$ ; the reduction in fringe spacing clearly indicates that the droplet has lost some of its water content through evaporation but has not frozen. Figure 5c provides images of the scattered light recorded immediately after trapping (0.0 s) and 5.0 s after injection for a frozen PWW droplet at  $-24.2^{\circ}\text{C}$ , both phase functions are irregular indicating that this droplet was frozen almost instantaneously within the trap. Figure 5d shows the phase functions of a trapped PWW 0.4 and 2.6 s after injection; the first phase function is regular and the second is irregular indicating that a freezing event happened after a short period of evaporation. Figure 5e provides the phase functions, at 0 and 60 s after injection, for a PWW which freezes instantaneously at  $-32.2^{\circ}\text{C}$ .

To test the freezing efficiency of PWW solution droplets, experiments were performed at ten different temperatures. The temperature dependent freezing fractions ( $f_{ice}$ ) of the PWW droplets, is calculated using Eq. (3).

$$f_{ice} = \frac{N_f}{N_0} \quad (3)$$

Where  $N_f$  is the number of PWW droplets that freeze, and  $N_0$  is the total number of PWW droplets.

The ice freezing fraction of droplets initially generated from a  $5 \text{ mg ml}^{-1}$  PWW solution is shown in Fig. 7. There is a clear increasing trend in the probability of PWW freezing as the temperature decreases. The freezing fraction increases rapidly from 0 to 0.85 as the temperature is lowered from  $-20.50 (\pm 0.65)$  to  $-22.45 (\pm 0.65) ^\circ\text{C}$ , and the frozen fraction reaches unity at temperatures  $\geq -27.5 (\pm 0.5) ^\circ\text{C}$ . The results of Pummer et al. (2012) and Pummer et al. (2013), which are presented in Augustin et al. (2013), are also shown in Fig. 7. These studies used a microscope equipped with a cryostage to investigate PWW emulsions of Silver birch (*Betula pendula*) (Pummer et al., 2012; Pummer, 2013; Augustin et al., 2013). The CEDB data using  $5 \text{ mg ml}^{-1}$  water birch (*Betula fontinalis occidentalis*) pollen PWW samples show a similar temperature dependent trend in  $f_{ice}$  to the  $50 \text{ mg ml}^{-1}$  *Betula pendula* PWW droplets. Both the  $f_{ice}$  values for these two different species increase rapidly, from an initial value of  $\sim 0$  to 1, in the relatively small temperature range of  $\sim 5 ^\circ\text{C}$ . The  $0.1 \text{ mg ml}^{-1}$  *Betula pendula* PWW droplets also have a similar shaped  $f_{ice}$  curve to the CEDB results but show subtle differences in freezing ability, compared to both the  $5 \text{ mg ml}^{-1}$  *Betula fontinalis occidentalis* sample and  $50 \text{ mg ml}^{-1}$  *Betula pendula* sample, with  $f_{ice}$  only reaching a value of  $\sim 0.9$  before the onset of homogenous nucleation at  $\sim 37.5 ^\circ\text{C}$ .

The similarity between the freezing curves of the two different pollen species from the same genus is intriguing; it suggests that the component(s) of PWW responsible for IN activity is common to the *Betula* genus. It should be noted that the pollen grains of both silver birch and water birch have very similar shapes with the characteristic raised pore

## A new electrodynamic balance design for low temperature studies

H.-J. Tong et al.

Title Page

Abstract

Introduction

Conclusions

References

Tables

Figures

◀

▶

◀

▶

Back

Close

Full Screen / Esc

Printer-friendly Version

Interactive Discussion



## A new electrodynamic balance design for low temperature studies

H.-J. Tong et al.

Title Page

Abstract

Introduction

Conclusions

References

Tables

Figures

◀

▶

◀

▶

Back

Close

Full Screen / Esc

Printer-friendly Version

Interactive Discussion



structure of the *Betula* genus, but it seems unlikely that these macro features of the pollen structure will have significant influence on the freezing ability on the filtered birch PWW. It has been shown that saccharides, lipids and proteins are easily removed from pollen particles via aqueous extraction (Pummer et al., 2013). It has been suggested that the IN ability of birch pollen PWW is not due to proteinaceous compounds but rather sugar-like macromolecules with masses between 100 and 300 kDa (Pummer et al., 2012).

The differences between the  $f_{ice}$  values of different species are likely due to the different concentrations of the extractable compounds. These differences can even occur across samples from the same genus and species but from different geographical regions (Augustin et al., 2013). We speculate that the yellow colour of the water birch PWW solution maybe indicates that it contains a high concentration of carotenoids, which may be one of the compounds that could influence the immersion freezing of PWW. It is possible that differences between the CEDB and cryostage measurement techniques may also influence the observed differences: the CEDB measurement used monodisperse ( $\sim 30\ \mu\text{m}$  diameter) sized PWW droplets, as opposed to the polydisperse PWW droplet size distribution (10–200  $\mu\text{m}$  diameter) of the cryostage experiments by Pummer et al. (2012, 2013). Secondly the PWW droplets in the CEDB are charged and cooled over a different timescale compared to the cryostage experiments. Finally the contact free nature of the CEDB may influence the outcome.

The experimental results presented in this study, in combination with other literature (Pummer et al., 2012; Augustin et al., 2013), indicate that birch PWW droplets are active in the immersion mode of freezing at relatively warm temperatures. However the freezing temperatures are lower than that observed for birch (*Betula alba*) pollen grains in the contact, immersion and condensation modes of freezing (Diehl et al., 2001, 2002). The IN activity behaviour shown by the birch PWW suggests significant potential for cloud formation and precipitation especially due to the wide geographical extent of birch.

## 4 Conclusions

This paper introduces a new design of CEDB. Furthermore it reports the initial applications of this CEDB to measure the evaporation kinetics and freezing properties of SWD. Accurate size and phase determination of the single levitated SWD was characterized via measurement of the Mie scattering signal. The rate of evaporation of SWD in a dry gaseous environment was determined, in the temperature range from  $-5$  to  $-34.5$  °C and the current setup allows the freezing experiments to be performed within a time window of up to one minute dependent on temperature. The phase transition of the PWW particle from liquid to frozen solid, and hence the freezing efficiency of PWW, was characterized through the loss of the regular Mie scattering signal from the levitated droplet. From this data, the statistical freezing fractions of PWW droplets were obtained in the temperature range:  $-4.5$  to  $-40$  °C. It was found that that PWW from water birch (*Betula fontinalis occidentalis*) pollen, in common with other *Betula* species (Pummer et al., 2012; Augustin et al., 2013) is IN active in the immersion freezing mode at relatively warm temperatures:  $-22$  °C and below. The evaporation and freezing results from this study illustrate the versatility of the new CEDB system for studying subzero phenomena in a contact free technique. The CEDB instrument will be used in future experiments to study a range of freezing phenomena and their implications for atmospheric ice nucleation.

**Acknowledgements.** This study was supported by NERC via the ACID-PRUF consortium grant (NE/I020105/1). We thank Jonathan Reid and James Davis for providing detailed information about their EDB design. We thank Thomas Leisner for good advice and providing the opportunity to visit his EDB laboratory. We thank Hinrich Grothe and Bernhard Pummer for provision of their PWW data sets.

## A new electrodynamic balance design for low temperature studies

H.-J. Tong et al.

Title Page

Abstract

Introduction

Conclusions

References

Tables

Figures

◀

▶

◀

▶

Back

Close

Full Screen / Esc

Printer-friendly Version

Interactive Discussion



## References

- Atkinson, J. D., Murray, B. J., Woodhouse, M. T., Whale, T. F., Baustian, K. J., Carslaw, K. S., Dobbie, S., O'Sullivan, D., and Malkin, T. L.: The importance of feldspar for ice nucleation by mineral dust in mixed-phase clouds, *Nature*, 498, 355–358, 2013.
- 5 Augustin, S., Wex, H., Niedermeier, D., Pummer, B., Grothe, H., Hartmann, S., Tomsche, L., Clauss, T., Voigtländer, J., Ignatius, K., and Stratmann, F.: Immersion freezing of birch pollen washing water, *Atmos. Chem. Phys.*, 13, 10989–11003, doi:10.5194/acp-13-10989-2013, 2013.
- Aylor, D. E.: Settling speed of corn (*Zea mays*) pollen, *J. Aerosol Sci.*, 33, 1601–1607, 2002.
- 10 Cantrell, W. and Heymsfield, A.: Production of ice in tropospheric clouds: a review, *B. Am. Meteorol. Soc.*, 86, 795–807, 2005.
- Choi, M. Y. and Chan, C. K.: The effects of organic species on the hygroscopic behaviors of inorganic aerosols, *Environ. Sci. Technol.*, 36, 2422–2428, 2002.
- Crawford, I., Möhler, O., Schnaiter, M., Saathoff, H., Liu, D., McMeeking, G., Linke, C., Flynn, M., Bower, K. N., Connolly, P. J., Gallagher, M. W., and Coe, H.: Studies of propane flame soot acting as heterogeneous ice nuclei in conjunction with single particle soot photometer measurements, *Atmos. Chem. Phys.*, 11, 9549–9561, doi:10.5194/acp-11-9549-2011, 2011.
- 15 Creamean, J. M., Suski, K. J., Rosenfeld, D., Cazorla, A., DeMott, P. J., Sullivan, R. C., White, A. B., Ralph, F. M., Minnis, P., Comstock, J. M., Tomlinson, J. M., and Prather, K. A.: Dust and biological aerosols from the Sahara and Asia influence precipitation in the western US, *Science*, 339, 1572–1578, 2013.
- 20 Davis, E. J.: A history of single aerosol particle levitation, *Aerosol Sci. Tech.*, 26, 212–254, 1997.
- Davies, J. F., Haddrell, A. E., and Reid, J. P.: Time-Resolved Measurements of the Evaporation of Volatile Components from Single Aerosol Droplets, *Aerosol Sci. Tech.*, 46, 666–677, 2012.
- 25 Davies, J. F., Miles, R. E. H., Haddrell, A. E., and Reid, J. P.: Influence of organic films on the evaporation and condensation of water in aerosol, *P. Natl. Acad. Sci. USA*, 110, 8807–8812, 2013.
- 30 Deguillaume, L., Leriche, M., Amato, P., Ariya, P. A., Delort, A.-M., Pöschl, U., Chaumerliac, N., Bauer, H., Flossmann, A. I., and Morris, C. E.: Microbiology and atmospheric processes: chemical interactions of primary biological aerosols, *Biogeosciences*, 5, 1073–1084, doi:10.5194/bg-5-1073-2008, 2008.

## A new electrodynamic balance design for low temperature studies

H.-J. Tong et al.

Title Page

Abstract

Introduction

Conclusions

References

Tables

Figures

◀

▶

◀

▶

Back

Close

Full Screen / Esc

Printer-friendly Version

Interactive Discussion





---

## A new electrodynamic balance design for low temperature studies

H.-J. Tong et al.

---

Title Page

Abstract

Introduction

Conclusions

References

Tables

Figures

◀

▶

◀

▶

Back

Close

Full Screen / Esc

Printer-friendly Version

Interactive Discussion



- DeMott, P. J., Prenni, A. J., Liu, X., Kreidenweis, S. M., Petters, M. D., Twohy, C. H., Richardson, M. S., Eidhammer, T., and Rogers, D. C.: Predicting global atmospheric ice nuclei distributions and their impacts on climate, *P. Natl. Acad. Sci. USA*, 107, 11217–11222, 2010.
- Després, V. R., Nowoisky, J. F., Klose, M., Conrad, R., Andreae, M. O., and Pöschl, U.: Characterization of primary biogenic aerosol particles in urban, rural, and high-alpine air by DNA sequence and restriction fragment analysis of ribosomal RNA genes, *Biogeosciences*, 4, 1127–1141, doi:10.5194/bg-4-1127-2007, 2007.
- Diehl, K., Quick, C., Matthias-Maser, S., Mitra, S. K., and Jaenicke, R.: The ice nucleating ability of pollen, Part I: Laboratory studies in deposition and condensation freezing modes, *Atmos. Res.*, 58, 75–87, 2001.
- Diehl, K., Matthias-Maser, S., Jaenicke, R., and Mitra, S. K.: The ice nucleating ability of pollen: Part II. Laboratory studies in immersion and contact freezing modes, *Atmos. Res.*, 61, 125–133, 2002.
- Glantschnig, W. J. and Chen, S.-H.: Light scattering from water droplets in the geometrical optics approximation, *Appl. Optics*, 20, 2499–2509, 1981.
- Griffiths, P. T., Borlace, J.-S., Gallimore, P. J., Kalberer, M., Herzog, M., and Pope, F. D.: Hygroscopic growth and cloud activation of pollen: a laboratory and modelling study, *Atmos. Sci. Lett.*, 13, 289–295, 2012.
- Heinisch, C., Bakić, C., Damaschke, N., Petter, J., Tschudi, T., and Tropea, C.: Neue Paulfallengometrie Zur Fixierung Von Tropfen Und Partikeln In Gasströmungen Mit 360°-Zugang Für Laserdiagnostik, 14 Fachtagung Lasermethoden in der Strömungsmesstechnik, PTB, Braunschweig, 2.61–2.66, 2006.
- Heinisch, C., Wills, J. B. Reid, J. P., Tschudi, T., and Tropea, C.: Temperature measurement of single evaporating water droplets in a nitrogen flow using spontaneous Raman scattering, *Phys. Chem. Chem. Phys.*, 11, 9720–9728, 2009.
- Heise, H. A. and Heise, E. R.: The distribution of ragweed pollen and alternaria spores in the upper atmosphere, *J. Allergy*, 19, 403–407, 1948.
- Helbig, N., Vogel, B., Vogel, H., and Fiedler, F.: Numerical modelling of pollen dispersion on the regional scale, *Aerobiologia*, 3, 3–19, 2004.
- Hirschfelder, J. O., Curtiss, C. F., and Bird, R. B.: *Molecular theory of gases and liquids*, John Wiley & Sons, Inc., New York, 1954.

---

## A new electrodynamic balance design for low temperature studies

H.-J. Tong et al.

---

Title Page

Abstract

Introduction

Conclusions

References

Tables

Figures

◀

▶

◀

▶

Back

Close

Full Screen / Esc

Printer-friendly Version

Interactive Discussion



Hoffmann, N., Kiselev, A., Rzesanke, D., Duft, D., and Leisner, T.: Experimental quantification of contact freezing in an electrodynamic balance, *Atmos. Meas. Tech.*, 6, 2373–2382, doi:10.5194/amt-6-2373-2013, 2013a.

Hoffmann, N., Duft, D., Kiseleva, A., and Leisner, T.: Contact freezing efficiency of mineral dust aerosols studied in an electrodynamic balance: quantitative size and temperature dependence for illite particles, *Faraday Discuss.*, 165, 383–390, 2013b.

Hogan, R. J., Behera, M. D., O'Connor, E. J., and Illingworth, A. J.: Estimate of the global distribution of stratiform supercooled liquid water clouds using the LITE lidar, *Geophys. Res. Lett.*, 31, L05106, doi:10.1029/2003GL018977, 2004.

Holyst, R., Litniewski, M., Jakubczyk, D., Kolwas, K., Kolwas, M., Kowalski, K., Migacz, S., Palesa, S., and Zientara, M.: Evaporation of freely suspended single droplets: experimental, theoretical and computational simulations, *Rep. Prog. Phys.*, 76, 034601, doi:10.1088/0034-4885/76/3/034601, 2013.

Hoose, C., Kristjánsson, J. E., Burrows, S. M.: How important is biological ice nucleation in clouds on a global scale? *Environ. Res. Lett.*, 5, 024009, doi:10.1088/0034-4885/76/3/034601, 2010.

Hoose, C. and Möhler, O.: Heterogeneous ice nucleation on atmospheric aerosols: a review of results from laboratory experiments, *Atmos. Chem. Phys.*, 12, 9817–9854, doi:10.5194/acp-12-9817-2012, 2012.

Kanji, Z. A., Welti, A., Chou, C., Stetzer, O., and Lohmann, U.: Laboratory studies of immersion and deposition mode ice nucleation of ozone aged mineral dust particles, *Atmos. Chem. Phys.*, 13, 9097–9118, doi:10.5194/acp-13-9097-2013, 2013.

Knopf, D. A., Alpert, P. A., Wang, B., and Aller, J. Y.: Stimulation of ice nucleation by marine diatoms, *Nat. Geosci.*, 4, 88–90, 2011.

Koop, T., Luo, B., Tsias, A., and Peter, T.: Water activity as the determinant for homogeneous ice nucleation in aqueous solutions, *Nature*, 406, 611–614, 2000.

Krämer, B., Hübner, O., Vortisch, H., Wöste, L., and Leisner, T., Schwell, M., Rühl, E., and Baumgärtel, H.: Homogeneous nucleation rates of supercooled water measured in single levitated microdroplets, *J. Chem. Phys.*, 111, 6521–6527, 1999.

Krieger, U. K., Colberg, C. A., Weers, U., Koop, T., and Peter, T.: Supercooling of single  $\text{H}_2\text{SO}_4/\text{H}_2\text{O}$  aerosols to 158 K: no evidence for the occurrence of the octahydrate, *Geophys. Res. Lett.*, 27, 2097–2100, 2000.

**A new  
electrodynamic  
balance design for  
low temperature  
studies**

H.-J. Tong et al.

Title Page

Abstract

Introduction

Conclusions

References

Tables

Figures

◀

▶

◀

▶

Back

Close

Full Screen / Esc

Printer-friendly Version

Interactive Discussion

- Krieger, U. K., Marcolli, C., and Reid, J. P.: Exploring the complexity of aerosol particle properties and processes using single particle techniques, *Chem. Soc. Rev.*, 41, 6631–6662, 2012.
- Laaksonen, A., Talanquer, V., and Oxtoby, D. W.: NUCLEATION: measurements, theory, and atmospheric applications, *Annu. Rev. Phys. Chem.*, 46, 489–524, 1995.
- Ladino Moreno, L. A., Stetzer, O., and Lohmann, U.: Contact freezing: a review of experimental studies, *Atmos. Chem. Phys.*, 13, 9745–9769, doi:10.5194/acp-13-9745-2013, 2013.
- Lee, A. K. Y. and Chan, C. K.: Single particle Raman spectroscopy for investigating atmospheric heterogeneous reactions of organic aerosols, *Atmos. Environ.*, 41, 4611–4621, 2007.
- Lee, A. K. Y., Ling, T. Y., and Chan, C. K.: Understanding hygroscopic growth and phase transformation of aerosols using single particle Raman spectroscopy in an electrodynamic balance, *Faraday Discuss.*, 137, 245–263, 2008.
- Lee, J. W. L., Carrascón, V., Gallimore, P. J., Fuller, S. J., Björkegren, A., Spring, D. A., Pope, F. D., and Kalberer, K.: The effect of humidity on the ozonolysis of unsaturated compounds in aerosol particles, *Phys. Chem. Chem. Phys.*, 14, 8023–8031, 2012.
- Li, K.-Y., Tu, H., Ray, A. K.: Charge limits on droplets during evaporation, *Langmuir*, 21, 3786–3794, 2005.
- Lohmann, U. and Feichter, J.: Global indirect aerosol effects: a review, *Atmos. Chem. Phys.*, 5, 715–737, doi:10.5194/acp-5-715-2005, 2005.
- Mie, G.: Beiträge zur Optik Trüber Medien, Speziell Kolloidaler Metallösungen, *Ann. Phys.*, 25, 377–445, 1908.
- Miles, R. E. H., Reid, J. P., Riipinen, I.: Comparison of approaches for measuring the mass accommodation coefficient for the condensation of water and sensitivities to uncertainties in thermophysical properties, *J. Phys. Chem. A*, 116, 10810–10825, 2012.
- Möhler, O., DeMott, P. J., Vali, G., and Levin, Z.: Microbiology and atmospheric processes: the role of biological particles in cloud physics, *Biogeosciences*, 4, 1059–1071, doi:10.5194/bg-4-1059-2007, 2007.
- Moller, B., Rarey, J., and Ramjugernath, D.: Estimation of the vapour pressure of non-electrolyte organic compounds via group contributions and group interactions, *J. Mol. Liq.*, 143, 52–63, 2008.
- Murphy, B. D. and Koop, T.: Review of the vapour pressures of ice and supercooled water for atmospheric applications, *Q. J. Roy. Meteor. Soc.*, 131, 1539–1565, 2005.

---

**A new  
electrodynamic  
balance design for  
low temperature  
studies**H.-J. Tong et al.

---

Title Page

Abstract

Introduction

Conclusions

References

Tables

Figures

◀

▶

◀

▶

Back

Close

Full Screen / Esc

Printer-friendly Version

Interactive Discussion



- Murray, B. J., Wilson, T. W., Dobbie, S., Cui, Z., Sardar, Al-Jumur, S. M. R. K., Möhler, O., Schnaiter, M., Wagner, R., Benz, S., Niemand, M., Saathoff, H., Ebert, V., Wagner, S., and Kärcher, B.: Heterogeneous nucleation of ice particles on glassy aerosols under cirrus conditions, *Nat. Geosci.*, 3, 233–237, 2010.
- 5 Murray, B. J., O’Sullivan, D., Atkinson, J. D., and Webb, M. E.: Ice nucleation by particles immersed in supercooled cloud droplets, *Chem. Soc. Rev.*, 41, 6519–6554, 2012.
- Niedermeier, D., Hartmann, S., Shaw, R. A., Covert, D., Mentel, T. F., Schneider, J., Poulain, L., Reitz, P., Spindler, C., Clauss, T., Kiselev, A., Hallbauer, E., Wex, H., Miltenberger, K., and Stratmann, F.: Heterogeneous freezing of droplets with immersed mineral
- 10 dust particles – measurements and parameterization, *Atmos. Chem. Phys.*, 10, 3601–3614, doi:10.5194/acp-10-3601-2010, 2010.
- Parsons, M. T., Riffell, J. L., and Bertram, A. K.: Crystallization of aqueous inorganic-malonic acid particles: nucleation rates, dependence on size, and dependence on the ammonium-sulfate, *J. Phys. Chem. A*, 110, 8108–8115, 2006.
- 15 Pope, F. D.: Pollen grains are efficient cloud condensation nuclei, *Environ. Res. Lett.*, 5, 044015, doi:10.1088/1748-9326/5/4/044015, 2010.
- Pope, F. D., Dennis-Smith, B. J., Griffiths, P. T., Clegg, S. L., Cox, R. A.: Studies of single aerosol particles containing malonic acid, glutaric acid, and their mixtures with sodium chloride, I. Hygroscopic growth, *J. Phys. Chem. A*, 114, 5335–5341, 2010a.
- 20 Pope, F. D., Tong, H.-J., Dennis-Smith, B. J., Griffiths, P. T., Clegg, S. L., Reid, J. P., Cox, R. A.: Studies of single aerosol particles containing malonic acid, glutaric acid, and their mixtures with sodium chloride, II. Liquid-state vapor pressures of the acids, *J. Phys. Chem. A*, 114, 10156–10165, 2010b.
- Pope, F. D., Gallimore, P. J., Fuller, S. J., Cox, R. A., and Kalberer, M.: Ozonolysis of maleic acid aerosols: initial results on aerosol hygroscopicity and volatility, *Environ. Sci. Technol.*, 44, 6656–6660, 2010c.
- 25 Pöschl, U.: Atmospheric aerosol: composition, transformation, climate and health effects, *Angew. Chem. Int. Ed.*, 44, 7520–7540, 2005.
- Pratt, K. A., DeMott, P. J., French, J. R., Wang, Z., Westphal, D. L., Heymsfield, A. J., Twohy, C. H., Prenni, A. J., and Prather, K. A.: In situ detection of biological particles in cloud ice-crystals, *Nat. Geosci.*, 2, 398–401, 2009.
- 30

## A new electrodynamic balance design for low temperature studies

H.-J. Tong et al.

Title Page

Abstract

Introduction

Conclusions

References

Tables

Figures

◀

▶

◀

▶

Back

Close

Full Screen / Esc

Printer-friendly Version

Interactive Discussion



Prenni, A. J., Petters, M. D., Kreidenweis, S. M., Heald, C. L., Martin, S. T., Artaxo, P., Garland, R. M., Wollny, A. G., and Pöschl, U.: Relative roles of biogenic emissions and Saharan dust as ice nuclei in the Amazon basin, *Nat. Geosci.*, 2, 401–404, 2009.

Pruppacher, H. R. and Klett, J. D.: *Microphysics of Clouds and Precipitation*, Atmospheric and Oceanographic Sciences Library, Kluwer Academic Press, Dordrecht, the Netherlands, 1997.

Pummer, B. G.: Ice nucleation activity of pollen and fungal spores, Ph.D. Dissertation, Technische Universität Wien, 2013.

Pummer, B. G., Bauer, H., Bernardi, J., Bleicher, S., and Grothe, H.: Suspendable macromolecules are responsible for ice nucleation activity of birch and conifer pollen, *Atmos. Chem. Phys.*, 12, 2541–2550, doi:10.5194/acp-12-2541-2012, 2012.

Pummer, B. G., Bauer, H., Bernardi, J., Chazallon, B., Facq, S., Lendl, B., Whitmore, K., and Grothe, H.: Chemistry and morphology of dried-up pollen suspension residues, *J. Raman Spectrosc.*, 44, 1654–1658, 2013.

Rauber, R. M. and Tokay, A.: An explanation for the existence of supercooled water at the top of cold clouds, *J. Atmos. Sci.*, 48, 1005–1023, 1991.

Rosenfeld, D. and Woodley, W. L.: Deep convective clouds with sustained supercooled liquid water down to  $-37.5^{\circ}\text{C}$ , *Nature*, 405, 440–442, 2000.

Rousseau, D.-D., Duzer, D., Cambon, G., Jolly, D., Poulsen, U., Ferrier, J., Schevin, P., and Gros, R.: Long distance transport of pollen to Greenland *Geophys. Res. Lett.*, 30, 1765, doi:10.1029/2003GL017539, 2003.

Sassen, K. Highly supercooled cirrus cloud water: confirmation and climatic implications, *Science*, 227, 411–413, 1985.

Schäppi, G. F., Taylor, P. E., Pain, M. C. F., Cameron, P. A., Dent, A. W., Staff, I. A., and Suphioglu, C.: Concentrations of major grass group 4 allergens in pollen grains and atmospheric particles: implications for hay fever and allergic asthma sufferers sensitized to grass pollen allergens, *Clin. Exp. Allergy*, 29, 633–641, 1999.

Seinfeld, J. H., Pandis, S. N.: *Atmospheric Chemistry and Physics: From Air Pollution to Climate Change*, Wiley, New York, 1998.

Shaw, R. A., Lamb, D., and Moyle, A. M.: An electrodynamic levitation system for studying individual cloud particles under upper-tropospheric conditions, *J. Atmos. Ocean. Tech.*, 17, 940–948, 2000.

---

**A new  
electrodynamic  
balance design for  
low temperature  
studies**H.-J. Tong et al.

---

Title Page

Abstract

Introduction

Conclusions

References

Tables

Figures

◀

▶

◀

▶

Back

Close

Full Screen / Esc

Printer-friendly Version

Interactive Discussion



Sofiev, M., Siljamo, P., Ranta, H., and Rantio-Lehtimäki, A.: Towards numerical forecasting of long-range air transport of birch pollen: theoretical considerations and a feasibility study, *Int. J. Biometeorol.*, 50, 392–402, 2006.

Soonsin, V., Zardini, A. A., Marcolli, C., Zuend, A., and Krieger, U. K.: The vapor pressures and activities of dicarboxylic acids reconsidered: the impact of the physical state of the aerosol, *Atmos. Chem. Phys.*, 10, 11753–11767, doi:10.5194/acp-10-11753-2010, 2010.

Stöckel, P., Weidinger, I. M., Baumgärtel, H., and Leisner, T.: Rates of homogeneous ice nucleation in levitated H<sub>2</sub>O and D<sub>2</sub>O droplets, *J. Phys. Chem. A*, 109, 2540–2546, 2005.

Stratmann, F., Kiselev, A., Wurzler, S., Wendisch, M., Heintzenberg, J., Charlson, R. J., Diehl, K., Wex, H., and Schmidt, S.: Laboratory studies and numerical simulations of cloud droplet formation under realistic supersaturation conditions, *J. Atmos. Ocean. Tech.*, 21, 876–887, 2004.

Svensson, E. A., Delval, C., von Hessberg, P., Johnson, M. S., and Pettersson, J. B. C.: Freezing of water droplets colliding with kaolinite particles, *Atmos. Chem. Phys.*, 9, 4295–4300, doi:10.5194/acp-9-4295-2009, 2009.

Swanson, B. D., Bacon, N. J., Davis, E. J., and Baker, M. B.: Electrodynamic trapping and manipulation of ice crystals, *Q. J. Roy. Meteor. Soc.*, 125, 1039–1058, 1999.

Tang, I. N. and Munkelwitz, H. R.: Water activities, densities, and refractive indices of aqueous sulfates and sodium nitrate droplets of atmospheric importance, *J. Geophys. Res.*, 99, 18801–18808, 1994.

Tong, H.-J., Reid, J. P., Bones, D. L., Luo, B. P., and Krieger, U. K.: Measurements of the timescales for the mass transfer of water in glassy aerosol at low relative humidity and ambient temperature, *Atmos. Chem. Phys.*, 11, 4739–4754, doi:10.5194/acp-11-4739-2011, 2011.

Vortisch, H., Krämer, B., Weidinger, I., Wöste, L., Leisner, T., Schwell, M., Baumgärtel, H., and Rühl, E.: Homogeneous freezing nucleation rates and crystallization dynamics of single levitated sulfuric acid solution droplets, *Phys. Chem. Chem. Phys.*, 2, 1407–1413, 2000.

Yttri, K. E., Dye, C., and Kiss, G.: Ambient aerosol concentrations of sugars and sugar-alcohols at four different sites in Norway, *Atmos. Chem. Phys.*, 7, 4267–4279, doi:10.5194/acp-7-4267-2007, 2007.

Zhang, Y. H. and Chan, C. K.: Study of contact ion pairs of supersaturated magnesium sulfate solutions using Raman scattering of levitated single droplets, *J. Phys. Chem A*, 104, 9191–9196, 2000.

Zobrist, B., Soonsin, V., Luo, B P., Krieger, U. K. Marcolli, C., Peter, T., and Koop, T.: Ultra-slow water diffusion in aqueous sucrose glasses, Phys. Chem. Chem. Phys., 13, 3514–3526, 2011.

## AMTD

7, 7671–7700, 2014

### A new electrodynamic balance design for low temperature studies

H.-J. Tong et al.

Title Page

Abstract

Introduction

Conclusions

References

Tables

Figures



Back

Close

Full Screen / Esc

Printer-friendly Version

Interactive Discussion

## A new electrodynamic balance design for low temperature studies

H.-J. Tong et al.

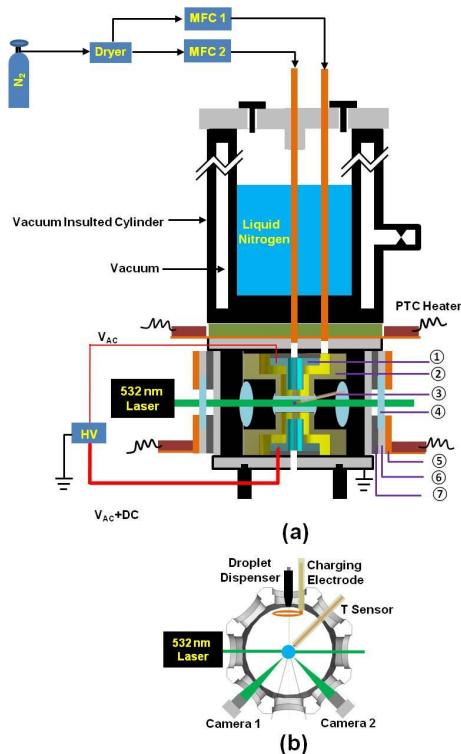


**Figure 1.** (a) Schematic diagram of the new CEDB system. ① Inner electrode. ② Outer electrode. ③ Thermocouple or relative humidity sensor. ④ Glass window. ⑤ Heating jacket. ⑥ Holder for glass window. ⑦ Rubber insulator. (b) The top view of the schematic diagram of optical design, dispensing and charging devices, and the thermocouple within the CEDB system. Cameras 1 and 2 are for droplet positioning and Mie scattering observation respectively.



## A new electrodynamic balance design for low temperature studies

H.-J. Tong et al.

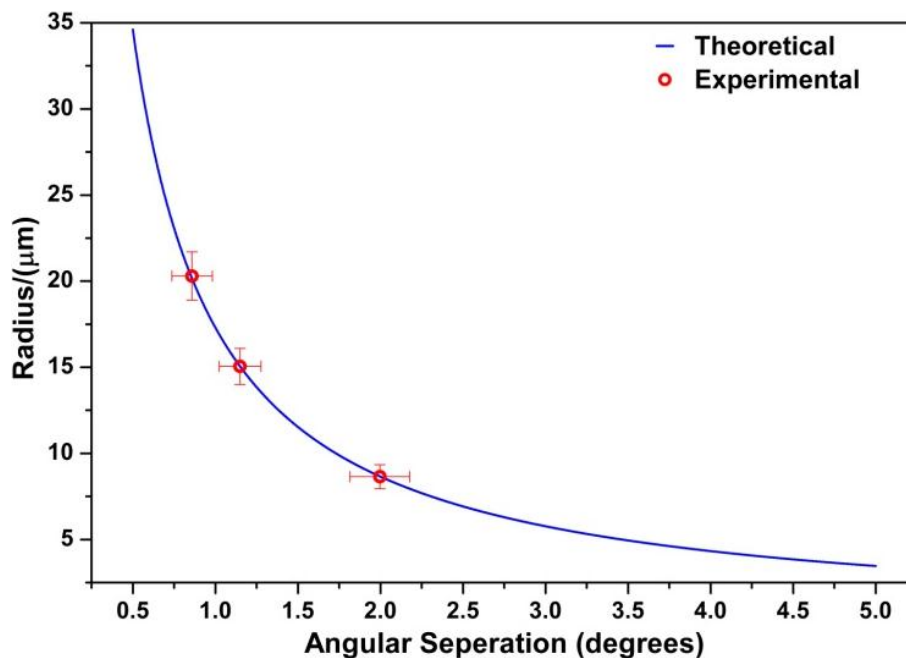


**Figure 2.** Measurement of particle radius by elastic Mie scattering. The size calibration is achieved using calibrated lime soda spheres. Blue line represents the calculated size based on the peak-to-peak spacing using Eq. (1). The experimental points (red circles) are the measured peak-to-peak separations in the recorded diffraction patterns against the quoted size. The uncertainty in the angular separation is the standard deviation ( $1\sigma$ ) in the measurement and the uncertainty in size is the standard deviation in particle size stated by the manufacturer.

[Title Page](#)[Abstract](#)[Introduction](#)[Conclusions](#)[References](#)[Tables](#)[Figures](#)[◀](#)[▶](#)[◀](#)[▶](#)[Back](#)[Close](#)[Full Screen / Esc](#)[Printer-friendly Version](#)[Interactive Discussion](#)

## A new electrodynamic balance design for low temperature studies

H.-J. Tong et al.

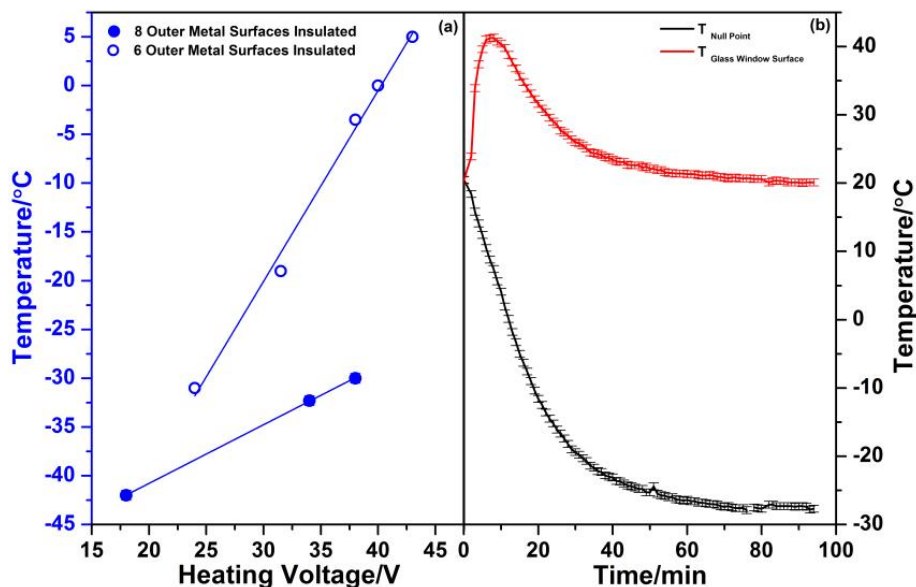


**Figure 3.** Temperature characterisation curves for the null point region of the CEDB. Two different insulation schemes allow to access different temperature ranges in the EDB. **(a)** Final temperature reached when 8 outer metal surfaces (blue solid circles) or 6 outer metal surfaces (blue circles) CEDB chamber vs. heating voltage. **(b)** An example of glass window surface (red line) and null point (black line) temperature to reach  $-28^{\circ}\text{C}$  with 24 V heating voltage.

## A new electrodynamic balance design for low temperature studies

H.-J. Tong et al.

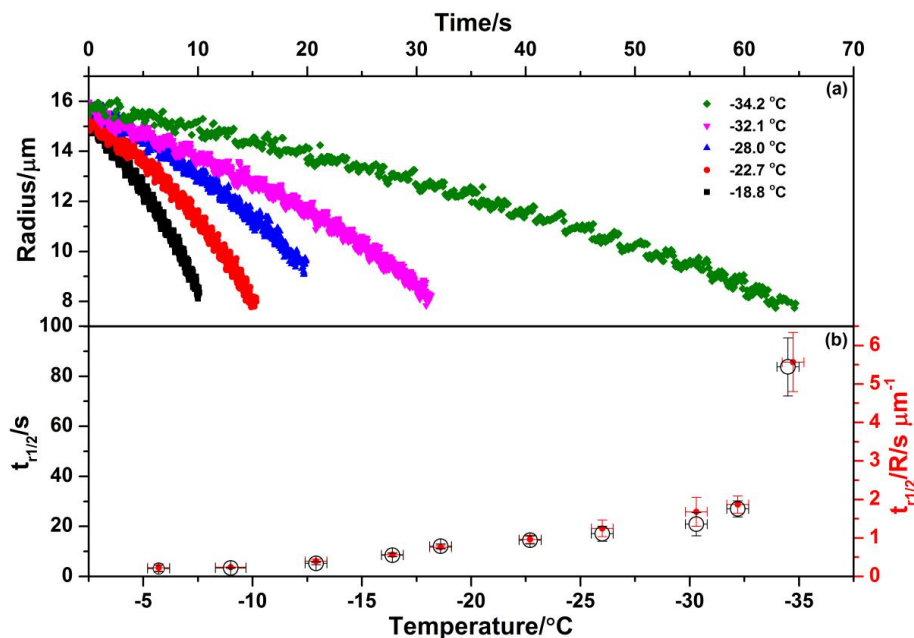


**Figure 4.** (a) Example evaporation decay traces of SWD at five different sub-zero temperatures. (b)  $t_{r1/2}$  of SWDs at 10 different temperatures (black circles), and the ratio of  $t_{r1/2}$  to radius ( $t_{r1/2}/R$ ) estimated for the change of SWD for a series of temperature measurements (red dots). The temperature error is the value stated by the manufacturer. The y-error for the  $t_{r1/2}$  and  $t_{r1/2}/R$  is the standard deviation of the measurement. At least three individual experiments at each temperature were conducted.

## A new electrodynamic balance design for low temperature studies

H.-J. Tong et al.

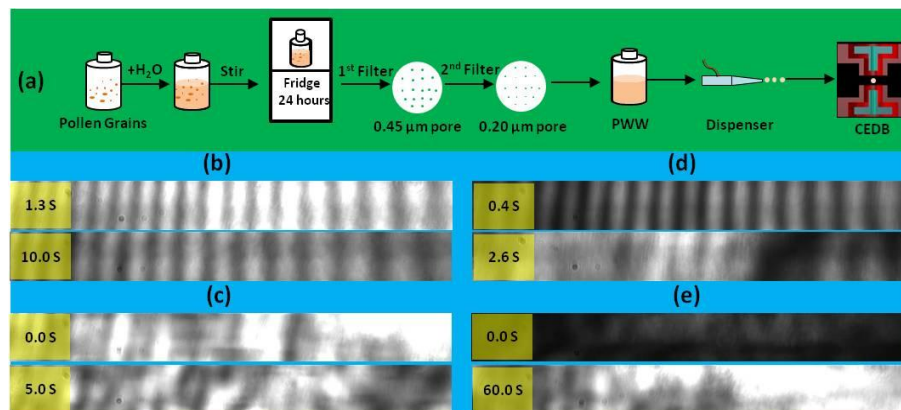


**Figure 5.** Extraction procedure and example phase dependent elastic Mie scattering images. **(a)** Cartoon of extraction procedure of PWW solutions. **(b)** The phase function of an evaporating PWW particle at  $-21.8^{\circ}\text{C}$  and recorded at 1.3 (top) and 10.0 s (bottom). **(c)** The irregular phase functions of a PWW particle that froze immediately after injection at  $-24.2^{\circ}\text{C}$ . **(d)** The recorded phase functions of a PWW particle that froze after a very short delay at  $-24.2^{\circ}\text{C}$ . **(e)** The irregular phase functions of a PWW particle that froze immediately after injection at  $-32.2^{\circ}\text{C}$ .

Title Page

Abstract

Introduction

Conclusions

References

Tables

Figures

◀

▶

◀

▶

Back

Close

Full Screen / Esc

Printer-friendly Version

Interactive Discussion

## A new electrodynamic balance design for low temperature studies

H.-J. Tong et al.

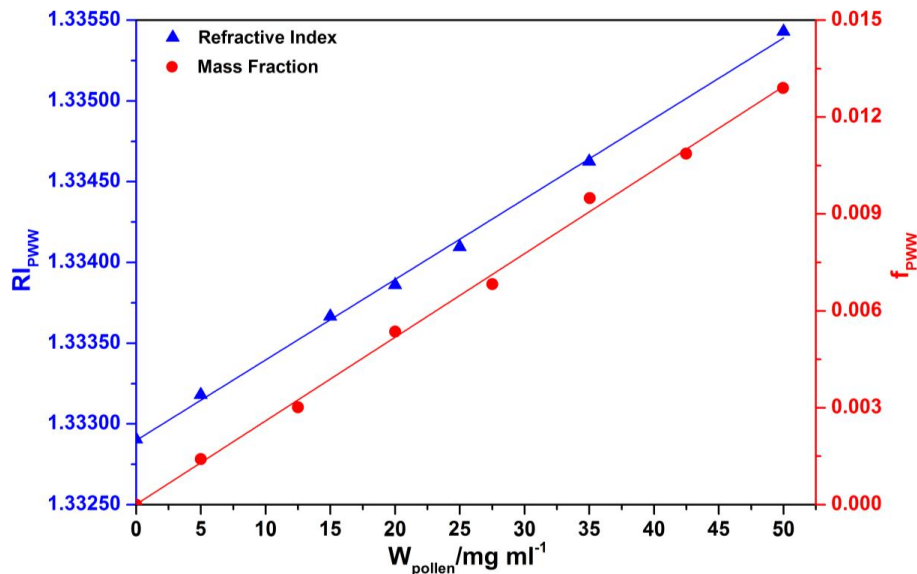


**Figure 6.** The mass fraction ( $f_{\text{PWW}}$ , red circles) and refractive index ( $RI_{\text{PWW}}$ , blue triangles) of PWW solutions vs. the pollen suspension concentration ( $W_{\text{pollen}}$ ). The red and blue lines are linear fits to the data with adjusted- $R^2$  values of 0.9969 and 0.9981, respectively.

[Title Page](#)
[Abstract](#)
[Introduction](#)
[Conclusions](#)
[References](#)
[Tables](#)
[Figures](#)
[Back](#)
[Close](#)
[Full Screen / Esc](#)
[Printer-friendly Version](#)
[Interactive Discussion](#)

## A new electrodynamic balance design for low temperature studies

H.-J. Tong et al.

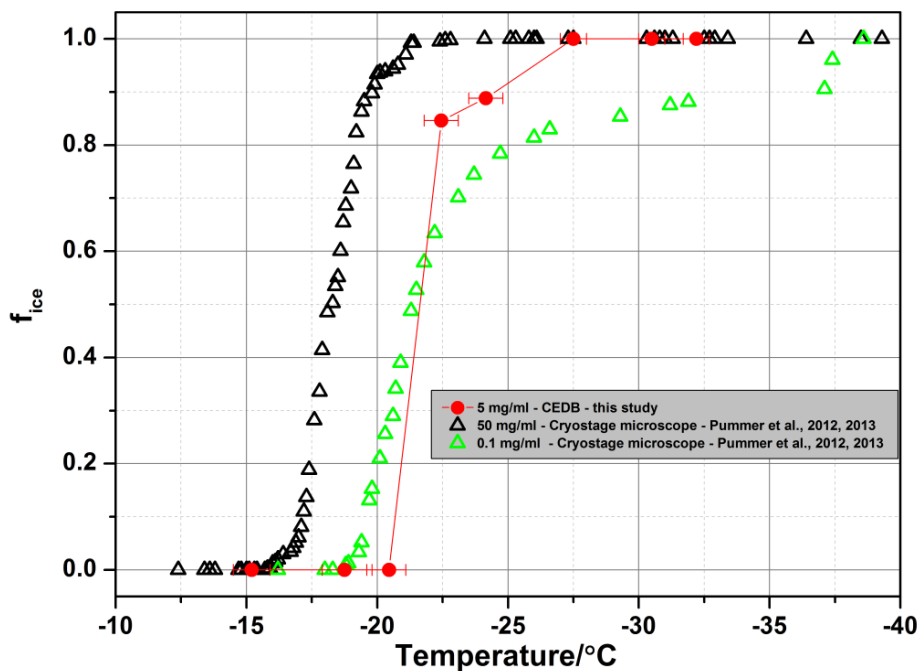


**Figure 7.** The temperature dependent freezing fraction ( $f_{ice}$ ) of birch PWW droplets. Data from this study (*Betula fontinalis occidentalis*, CEDB) is compared to the data reported in Augustin et al. (2013) for *Betula pendula* obtained using a cryostage microscope. The temperature error bar is calculated using both the stated probe accuracy from the manufacturer plus the fluctuation of experimental temperature for each data point.